Available online at www.sciencedirect.com

ScienceDirect

Procedia Computer Science 200 (2022) 160–174

Procedia Computer Science

www.elsevier.com/locate/procedia

3rd International Conference on Industry 4.0 and Smart Manufacturing

An Evaluation Study of EMD, EEMD, and VMD For Chatter Detection in Milling

Pelin Seyrek[a], Batıhan Şener[a], A. Murat Özbayoğlu[b], Hakkı Özgür Ünver[a,*]

[a]*Department of Mechanical Engineering, TOBB University of Economics and Technology, Ankara, Turkey*
[b]*Department of Artificial Intelligence Engineering, TOBB University of Economics and Technology, Ankara, Turkey*

Abstract

In modern machining processes, chatter is an inherent phenomenon that hinders efficiency, productivity, and automation. Numerous methods have been proposed using analytical, computational, and artificial intelligence methods to detect and avoid chatter during milling. The vibration signals generated during machining are of non-stationary and non-linearity nature. Hence solely time or frequency domain analysis are not adequate methods for chatter detection. This study investigates the performance of more advanced mode decomposition methods and compares them. Three decomposition methods, namely, empirical mode decomposition (EMD), ensemble empirical mode decomposition (EEMD), and variational mode decomposition (VMD), are used to decompose and identify chatter frequency bands. After decomposition, Hilbert-Huang transform (HHT) was applied for visualization. The comparative results indicate that EEMD or VMD decomposition methods performed better than EMD for intelligent chatter detection.

Keywords: Milling, Chatter Detection, Empirical Mode Decomposition (EMD), Ensemble Empirical Mode Decomposition (EEMD), Variational Mode Decomposition (VMD)

1. Introduction

Advanced machine tools for the metal cutting industry possess advanced technology to increase production, efficiency, and automation for Industry 4.0. Milling is the most widely used machining process in many high-tech industries, such as aviation, medical, and automotive. Unlike the other machining processes, milling is prone to chatter as it is an interrupted cutting process. Chatter is observed in milling primarily due to increased natural frequency, chatter formation with the damping effect's wavelength, overlapping oscillation waves, change of cutting force, and normal force at each tooth stroke frequency. Tlusty examined regenerative chatter by using cutting force base calculated force and vibration simulations and constructed the theoretical stability lobes and regenerative chatter [1]. Altintas et al. identify regenerative chatter that occurs due to feedback excitation of wavy-cut surfaces to machine tool dynamics, resulting in amplifying specific frequency ranges, which can deter the operation's stability. Stability limits are defined by an additional analytical method based on dynamic milling formulation. This formulation is based on the regeneration of the chip thickness, variational directional factors, and machine tool structure interaction. It is vital to select the process parameters avoiding regenerative chatter to enable high material removal rates, avoiding complications, such as rapid tool wear, low surface quality, and tool breakage [2].

* Corresponding author. Tel.: +90-312-292-4261
E-mail address: hounver@etu.edu.tr

1877-0509
10.1016/j.procs.2022.01.215

Many scholars investigated machine tool dynamics. Butcher et al. used Chebyshev polynomials and the Chebyshev collocation points to stabilize the up and down milling process based on spindle speed and depth of cut [3]. Moghaddas et al. obtained and simulated a numerically nonlinear equation of motion by modeling the milling process with a time-periodic delay differential equation based on the constant depth of cut and spindle speed [4]. Moradi et al. presented the structural nonlinearity and nonlinear cutting forces by a dynamic model of the peripheral milling process using the multiple-scale approach as a perturbation technique [5]. Kiss et al. evaluated the dynamics of the beam type workpiece created with the Finite element model by considering the chatter and resonance conditions, which are unattainable in practice. Up milling and down milling operation results were compared with theoretical results depending on Spindle speed and tooth path. Non-stable chatter regions were determined based on the roughness measurements. MSLE (Maximum Surface Location Error) is used to determine the chatter [6].

Recently, the identification of chatter with statistical and machine learning methods for online monitoring of the processes has been gaining attention—these studies most commonly used signals from vibration, force, acoustics, and motor current sensors. Lamraoui et al. used the motor current signal to detect the chatter with Support Vector Machine (SVM). Firstly, statistical features (Root Means Square (RMS), Variance, Kurtosis, Crest Factor, Impulse Factor, Skewness, Peak Value, Clearance Factor and Shape Factor) are extracted, then calculated of these values entropies and classified with SVM based on the selected four features that have the highest entropy value. It is demonstrated that SVM has the least errors compared to MLP and RBF simultaneously [7]. Wojciechowski et al. determined the cutting process's stability using vibration signals with MLP [8]. Similarly, Kuljanic et al. extracted statistical features from wavelet decomposition of vibration signals and used Artificial Neural Network (ANN) to detect the chatter [9].

Signal feature extraction could be done by three methods: time domain, frequency domain, and time-frequency domain. Time-domain and frequency-domain use for the stationary signals. However, all machining processes generate non-stationary signals. It is necessary to use time-frequency techniques for these types of signals such as short-time Fourier transform, Wigner–Ville distribution, Gabor transform, wavelet transform, wavelet packet transform, Hilbert–Huang transform, high order spectral analysis, or bilinear transform. Wavelet packet transform is a high-resolution analysis that decomposes the signal simultaneously using the high pass and low pass. This transform decreases the noise of the signal at the same time. Penga et al. calculated energy and entropy values after wavelet packet transform, and the chatter is detected with Support Vector Classification (SVC). It is also determined that FFT of cutting force signals on x and y directions have additive frequencies near the natural frequency bands [10].

This paper investigates chatter detection with several empirical decomposition methods: Empirical Mode Decomposition (EMD), Ensemble Empirical Mode Decomposition (EEMD), and Variational Mode Decomposition (VMD) using vibration data from the half immersion slot milling process of Al-7075. These detection techniques have great potential for pre-processing data for deep learning algorithms, and the main objective of this work is to compare the performance of these methods for deep learning. Similarly, Liu et al. applied VMD to the signals and reconstructed by using the highest kurtosis value to select the most suitable Intrinsic Mode Functions (IMFs), and after the selection of the IMFs, energy, and entropy values were computed to identify chatter bands [11].

In our study, the signal was denoised using Wavelet Package Transformation (WPT). It was then decomposed into its intrinsic modes with EMD, EEMD, and VMD, followed by the Hilbert Huang transform (HHT) applied to selected IMFs. Similarly, Cao et al. used WPD and HHT for chatter detection. After applying the comb filter as a pre-process to the vibration signals to determine the chatter, Cao et al. decomposed the signals into their IMF with EEMD. They find that the first IMF has chatter information by viewing the energy ratios among the eight IMFs extracted [12, 13]. The complexity, spectral entropy, and FFTs of the selected IMF were computed. As the chatter level of the FFTs increases, the chatter frequencies increase was observed clearly, and the other calculated features increased as well. Yang et al. selected the components containing chatter information by decomposing the force signals with VMD and calculated approximate entropy values of these components to determine the online chatter [14].

2. Methods and experiment

2.1 Methods

2.1.1 Hilbert Huang transform

Data from either physical measurement have several problems as if they are from non-stationary and nonlinear processes. Under these circumstances, there are limited options to use for analysis. For the Fourier spectral analysis, stationarity is a requirement, and linearity is a must. Real-time signals from vibration sources are not linear or stationary. The Hilbert transform extracts the full energy–frequency-time distribution of the data, ideal for nonlinear and non-stationary signals. To decompose any non-stationary time series, EMD is one of the well-known decomposition methods defined by N.E.Huang [15]. Hilbert Huang Transform (HHT) takes place in two stages. First, the EMD process that provides the separation of the signals is applied. EMD separates signals into IMFs. The original signal refers to the sum of these separation results. Afterward, Hilbert Spectrum processing is performed using the decomposed signals as IMFs by Huang et al.. This spectrum analysis is similar to the Fourier expansion analysis compared to its constant frequencies and coefficients [16].

2.1.1.1 Empirical mode decomposition and ensemble empirical mode decomposition

By the process of empirical mode decomposition, IMFs are extracted based on the signal's local properties that make the instantaneous frequency meaningful. Instantaneous frequencies are necessary for the correct representation of nonlinear and non-stationary signals to get rid of harmonics. IMFs are defined as functions with the same number of zero-passes and symmetrical envelopes concerning local minimum and maximum. Until it reaches the specified stopping criteria, the signal is split into its IMFs and becomes separate components [15]. When the sub-signals and residual signals resulting from EMD are collected, the original signal can be obtained without losing information. EMD is not a technique used to filter the frequency bands like wavelets [16]. There can be only one extremum point between the two zero crossings of IMFs, as shown in Fig. 1 (a). An IMF is a function that satisfies two conditions within the entire data set; extrema and zero crossings' numbers must either equal or differ at most by one, and at any point, the mean value of the local minima and maxima envelope is zero. The local mean of the data being zero prevents the unwanted fluctuations that are induced by asymmetric waveforms in the instantaneous frequencies [17]. In the equation below, a signal is represented in terms of its IMFs. n^{th} number of IMF are reached at the end of the process. $x_n(t)$ is used to indicate the IMF with each n index number.

$$x(t) = \sum_n x_n(t) + r(t) \tag{1}$$

x(t): Original Signal

x_n(t): IMFs

r(t): Residual Signal

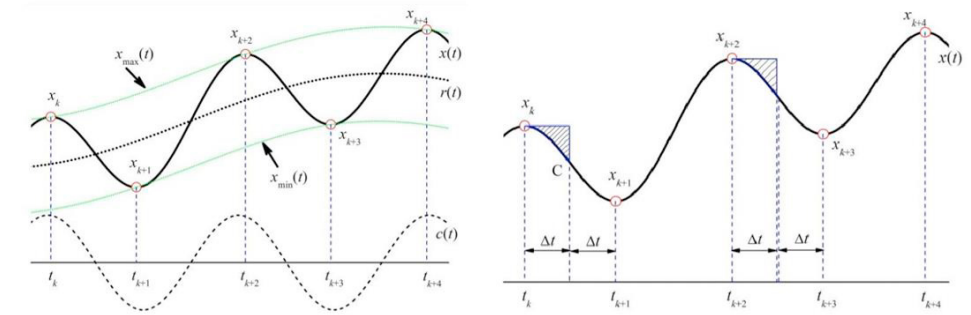

a) b)

Fig. 1. a) Sample signal for analysis b) Representation of integrals at different ranges [17]

As can be seen in Fig. 1, for two local minimum or maximum points and c(t) is zero as a function of oscillation with a mean value of zero. The following equation is theoretically the basis of the signal decomposition process, where r_0 term represents the initial residual of the process.

$$\int_{t_k}^{t_{k+2}} x(t)\,dt = \int_{t_k}^{t_{k+2}} c(t)\,dt + \int_{t_k}^{t_{k+2}} r(t)\,dt = \int_{t_k}^{t_{k+2}} r(t)\,dt = r_0(t_{k+2}) - r_0(t_k) \tag{2}$$

x(t): Non-stationary oscillated signal

c(t): Oscillation component

r(t): Residual signal

For $\Delta t = \frac{t_{k+1}-t_k}{2}$ shown in Fig. 1 (b), the following equation is obtained when one extreme point in two-time intervals is viewed over four points (k… k + 4), which are stated in Fig. 1 (b). This process demonstrates that the signal can be decomposed approximately using the local minimum and maximum points. Following equation gives the residual signal calculation due to local maximum, $x_{max}(t)$, and local minimum, $x_{max}(t)$, points.

$$r(t) = \frac{[x_{max}(t) + x_{min}(t)]}{2} \tag{3}$$

In the first stage of the EMD algorithm, the received signal is taken as a residual signal, and the local minimum and maximum values are calculated by the cubic spline method. Then, the mean values of minimum and maximum are found. The new component is obtained by subtracting this average signal calculated from the signal in the previous component. Then, the local minimum and maximum values are calculated again. The process is repeated until stopping criteria are satisfied. Each component whose local minimum, maximum and average values are calculated are recorded as an IMF signal. While the signal itself is initially received as a residual signal, in each subsequent iteration of the process, the residual signal is obtained by subtracting the IMF signal from the previous residual signal after the IMF is recorded and the process continues iteratively. The physical interpretation of sub-signals received with EMD cannot be guaranteed. Modes in IMFs can be mixed, as given in Fig. 2 (a). In the figure, the mode mixing problem in the first and second IMFs is visible. Empirical Mode Decomposition (EEED) was developed to solve this issue, as its results can be seen in Fig. 2 (b)[16].

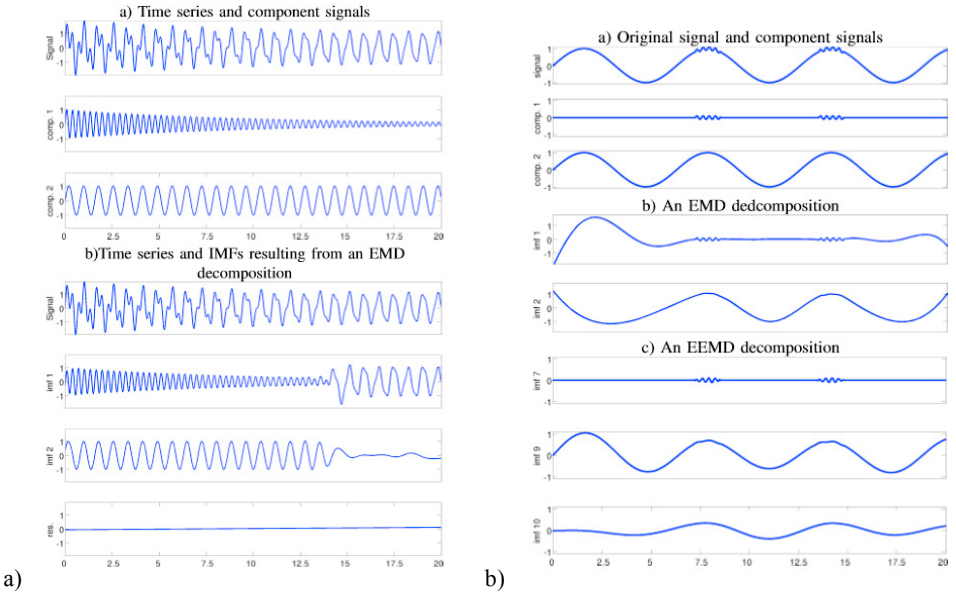

Fig. 2. (a) IMFs resolved by EMD with mode mixing (b) EMD and EEMD IMFs compared [16]

EEMD, created by developing the screening system by ensemble approach, was developed by Zhaohua Wu and Norden E. Huang. This decomposition method resolves the mode mixing problem, as shown in Fig. 2. (b). Correct analysis is made with the EEMD while mixing occurs in the EMD process. The approach consists of assembling a group of white noise added signals and treating the mean as the actual result. Hence weakness of EMD is fixed to reach better decomposition for making the results more interpretable [18, 30].

EEMD, a time-space analysis method, is used with the added white noise to get the more accurate and physical solutions, averaged out with sufficient number of trials. During the averaging process, only the persistent part survives. The added white noise provides a uniform reference frame in the time-frequency space. For this reason, the added noise collates the portion of the signal of comparable scale in one IMF. The principle of the EEMD is the added white noise. By this noise, the whole time-frequency space is populated uniformly with the constituting components of different scales. By adding the signal to this uniformly distributed white background, the bits of the signal of different scales are automatically projected onto proper scales of reference established by the white noise in the background. As a result of this process, noisy results can be produced by each trial. The ensemble mean of enough trials removes it. In the end, the only persistent part is the signal as more and more trials are added in the ensemble. The final standard deviation of errors can be calculated using the following equation [18, 19].

$$\varepsilon = \frac{A}{\sqrt{N}} \tag{4}$$

Where N is the number of ensemble members, A is the amplitude of the added noise, and ε is the final standard deviation of the error, which is defined as the difference between the input signal and the corresponding IMF(s).

2.1.1.2 Variational mode decomposition

VMD is an approach for adaptive and quasi-orthogonal signal decomposition. Multi-component signals are decomposed into several band-limited intrinsic mode functions by VMD [20]. To assess the bandwidth of a mode, the associated analytic signal is computed using the Hilbert transform to obtain a unilateral frequency spectrum for each mode that is presented by u_k. Then, the mode's frequency spectrum is shifted to "baseband" by mixing with an exponential tuned to the respective estimated center

frequency. Finally, the bandwidth is estimated through the H1 Gaussian smoothness of the demodulated signal. Mathematically, based on the squared L_2-norm of the gradient, VMD can be expressed as [21]:

$$\min_{u_k.\omega_n} \sum_{k=1}^{K} \| \partial_t \left[\left(\delta(t) + \frac{j}{\pi t} \right) \times u_k(t) \right] e^{-j\omega_n t} \|_2^2 \tag{5}$$

$$f = \sum_{k=1}^{K} u_k \tag{6}$$

u_k : Sub-signals

ω_n: Center Pulsation of Modes

f : Real valued signal

With the following equation, the solution of the minimization problem that given in the 5th equation is found in a sequence of iterative sub-optimizations. Given Lagrangian form includes frequencies as complex demonstration which consists of the imaginary parts ($j = \sqrt{-1}$). From the Tikhonov regularization formula, second term is the squared norm of current frequency minus f_0, The augmented Lagrangian can be written as:

$$\mathcal{L}(u_k, \omega_k, \lambda) = \alpha \sum_{\mathrm{k}} \| \partial_t \left[\left(\delta(t) + \frac{j}{\pi t} \right) * u_k(t) \right] e^{-j\omega_k t} \|_2^2 + \| f - \sum u_k \|_2^2 + \langle \lambda, f - \sum u_k \rangle \tag{7}$$

2.1.1.3 Hilbert spectrum

Hilbert spectrum is the second stage for the HHT. After signals decomposed with any method, the Hilbert spectrum is applied. Hilbert spectrum analysis is similar to the Fourier expansion analysis. This method uses instantaneous frequencies and coefficients instead of constant frequencies and coefficients and is used for the nonlinear experimental analysis for complex, variable time series. Characteristics of nonlinear and variable signals are achieved with EMD. Hilbert transform essentially calculates conjugate pairs of IMFs and P is the Cauchy principal. Calculations are given in the following equations [16].

$$H\{x_i(t)\} = \frac{1}{\pi} P \left\{ \int_{-\infty}^{\infty} \frac{x_i(\tau)}{(t-\tau)} d\tau \right\} \tag{8}$$

$$z_i(t) = x_i(t) + iH\{x_i(t)\} = a_i(t) e^{i\theta_i(t)} \tag{9}$$

$$a_i(t) = \sqrt{x_i^2(t) + H\{x_i(t)\}^2} \tag{10}$$

$$Q_i(t) = \arctan\left(\frac{H\{x_i(t)\}}{x_i(t)} \right) \tag{11}$$

Using the above equations, each IMF is expressed as in the equation below.

$$x_n(t) = \mathrm{Re}\left[a_n(t) e^{i \int w_n(t) dt} \right] \tag{12}$$

The Fourier Transform representation is as given by constants a_n and w_n in the equation below. Fourier transform can be applied to stationary and linear time series.

$$x(t) = \sum_{n=1}^{\infty} a_n e^{i\, w_n t} \tag{13}$$

IMF represents a generalized Fourier expansion, but the amplitude and the frequency modulations decomposed predominately. The variable amplitude and the instantaneous frequency improved the efficiency of the expansion. Thus, this process can be applied to non-stationary data [14].

2.1.2 Wavelet packet denoising

Complex signals contain different time-frequency structures that provide the exploration of time-frequency representation with adaptive properties. Wavelet packages separate the frequencies in various sizes as the multi-resolution analysis that have the same computation for wavelet packet coefficients with a filter bank. Multi-resolution analysis and wavelet packet transform commonly used orthogonal decompositions. With low and high pass filter (two-channel filter bank), The wavelet packet transform decomposed the signals orthogonally. Wavelet decomposition algorithms include hard or soft thresholding and fixed or level-dependent thresholds. For different applications, the optimal wavelet thresholding method should be considered carefully [22]. Since Discrete Wavelet Transform is not enough in most applications, Continuous Wavelet Packet Decomposition is required. There may be many fields where wavelet packet decomposition is used as GPS static high-precision positioning [23], image processes [24]. Noise removal with Wavelet Packet is performed in four steps as given below.

2.1.2.1 Wavelet transform

Continuous wavelet transform (CWT) is defined by Daubechies with the following equations, where a and b are scaling and translation factors [25].

$$W\,x(a,b) = \int_{-\infty}^{+\infty} x(t)\psi_{a,b}(t)d\,t \tag{14}$$

Another version of the wavelet function is obtained by the following equation, where a and b are real numbers and a is nonzero. As the number increases, the low-frequency components of the signal are analyzed. As the number of a becomes smaller, the high-frequency components of the signal are analyzed.

$$\psi_{a,b}(t) = |a|^{-\frac{1}{2}}\psi\left(\frac{t-b}{a}\right) \tag{15}$$

Discrete Wavelet Transform obtained by choosing constants as $a = a_0^m \; and \; b = nb_0a_0^m$. $(m, n = 0, \pm1, \pm2 \ldots)$. For DWT and CWT, $\int \psi(t)d\,t$ must be zero.

$$Wx(m,n) = \int_{-\infty}^{+\infty} x(t)\psi_{m,n}(t)d\,t = a_0^{-m/2}\int_{-\infty}^{+\infty} x(t)\psi(a_0^{-m}t - nb_0)d\,t \tag{16}$$

Discrete wavelets consist of $a_0 = 2\;ve\;b_0 = 1$. The following equation is used in the orthonormal-based multi-resolution analysis.

$$\psi_{\{m,n\}}(t) = 2^{-\frac{m}{2}} * \psi(2^{-m} * t - n) \tag{17}$$

In Discrete wavelet analysis, the x (t) decomposition is performed with the following formula.

$$x(t) = \sum_{j=1}^{K}\sum_{k=-\infty}^{\infty} d_j(k)\psi_{j,k}(t) + \sum_{k=-\infty}^{\infty} a_K(k)\phi_{K,k}(t) \tag{18}$$

$\psi_{j,k}(t)$: Discrete Analysis of Wavelets

$\phi_{K,k}(t)$: Discrete Scaling Function

$d_j(k)$: Wavelet Coefficients (Scaled with 2^j)

$a_K(k)$: Approximated Signal (Scale coefficients) (Scaled with 2^K)

2.1.2.2 Wavelet packet decomposition

Wavelet packet is used for a better representation of frequency decomposition. Four-level wavelet packet decomposition is shown in Fig. 3. The coefficients are obtained by dividing the signal into two as high and low pass at each level. The signal is obtained with an inverse wavelet transform in the last step [23].

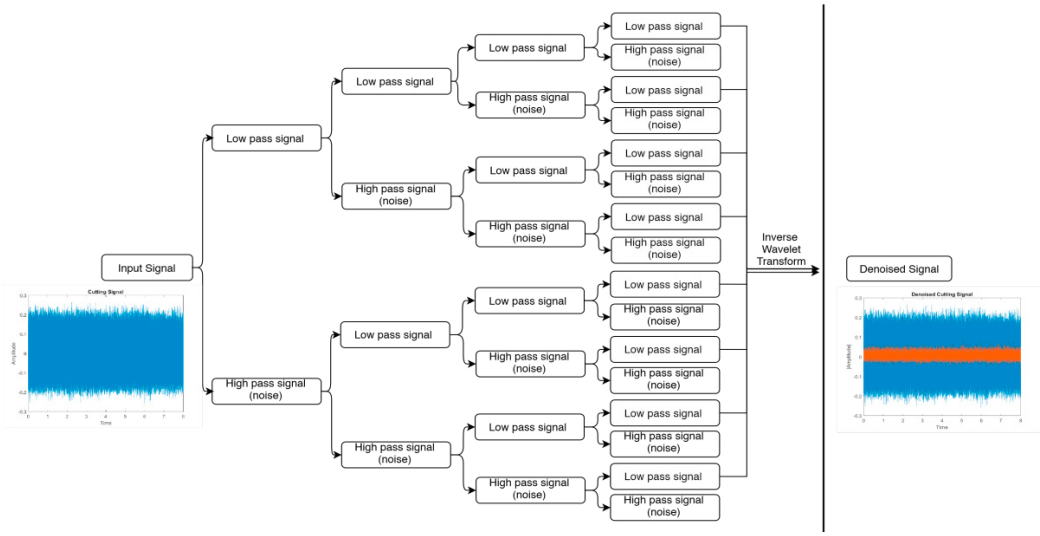

Fig. 3. Four level wavelet packet decomposition

Wavelet packet analysis corrects low-frequency resolution in the high-frequency part. It performs an orthogonal decomposition. It extracts signal characteristics in all frequency bands, especially high ones. It divides the signal into different frequency bands at different levels. When it is sufficiently low, the starting and ending frequencies can be obtained. In this way, noise can be extracted from the original signal [26]. To calculate the threshold values, the magnitudes of transform coefficients (O_l) are compared with the λ limit. Calculations as hard, soft and mid thresholding can be calculated as given below [27].

Hard:

$$O_l = \begin{cases} 0, & if\ |O_l| \le \lambda\ ; \\ O_l, & otherwise. \end{cases} \tag{19}$$

Soft:

$$O_l = sign\{O_l\}(|O_l| - \lambda)_* \tag{20}$$

Where,

$$sign\{O_l\} \equiv \begin{cases} +1, & if\ O_l > 0; \\ 0, & if\ O_l = 0; \\ -1, & if\ O_l < 0. \end{cases} \quad \text{And} \quad (x)_* = \begin{cases} x, & if\ x \ge 0\ ; \\ 0, & if\ x < 0. \end{cases}$$

Mid:

$$O_l = sign\{O_l\}(|O_l| - \lambda)_{**} \tag{21}$$

Where,

$$(|O_l| - \lambda)_{**} \equiv \begin{cases} 2(|O_l| - \lambda)_*, & if\ |O_l| < 2\lambda\ ; \\ |O_l|, & otherwise. \end{cases}$$

The following equation is used to determine the threshold value [28].

$$\lambda = \sigma\sqrt{2\log l} \tag{22}$$

σ: Noise Level

$$\sigma = \frac{Median\left\{\left|O_{\{j-1,k\}}\right|: 0 \le k < \frac{l}{2}\right\}}{0{,}6745} \tag{23}$$

At the end of this process, reverse wavelet transform is applied, and a noiseless signal is obtained by reconstructing the new noiseless wavelet coefficients that are obtained using the threshold values [23].

The experiments were carried out on a DMG-MORI® DMU 65 Monoblock 5-axis machine tool. Details of the experimental setup and technical features of this machine toll are shown in Table 1. Experimental conditions. Acceleration signals were collected from an accelerometer placed on the spindle. The sensor is connected to NI (National Instruments) 9234 data collection module on the NI DAQ Platform to realize raw data collection. During the experiment, cooling liquid was not used to prevent the influence of the liquid on the process.

Table 1. Experimental conditions

Machine tool model	DMG-MORI DMU Monoblock 65	
Working area (mm)	735x650x560	
Spindle power (kW)	37	
Axis	5-axis	
Tool specifications	Diameter	10 mm
	Flute Length	22 mm
	Total Length	72 mm
	Number of Flutes	3
	Rake angle	6˚
	Helix angle	30˚
Workpiece material	Al 7075	
Tool material	Tungsten Carbide	

The experimental collection setup consisting of the module and computer to which the sensors are connected is shown in Fig. 4 Labview™ application was used on the software side, enabling data acquisition from NI modules for further processing with Matlab™. The cuts were half immersion slot milling with a maximum revolution speed of 16,000 rpm.

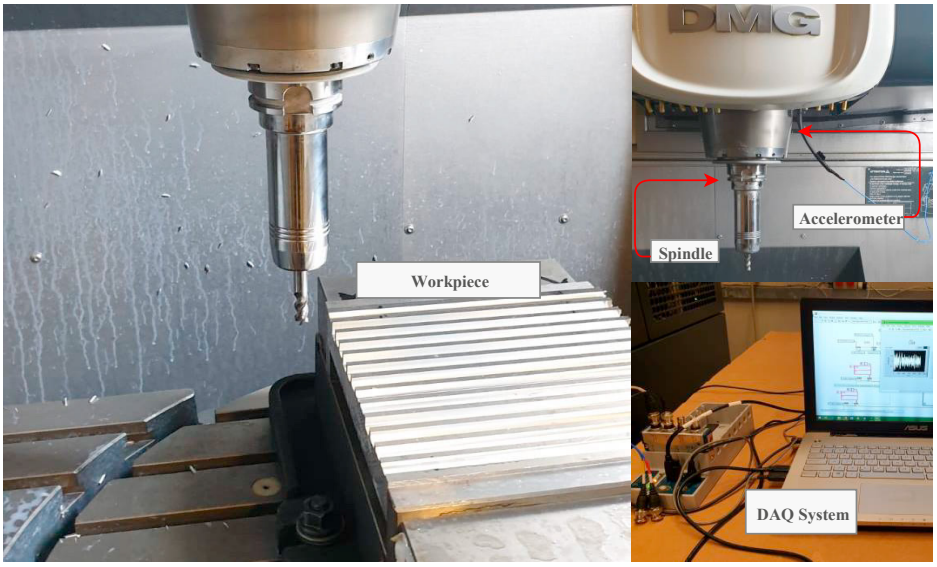

Fig. 4. Experimental setup

3. Results and discussion

Using the experimental frequency response functions, time-domain simulation was performed with MATLAB using Tlusty's method. Stability lobes are created via a heatmap by calculating the RMS values of simulated vibration data. The resulting stability lobe heat map is given in Fig. 5. The points marked in the figure are the cuts, which results will be examined.

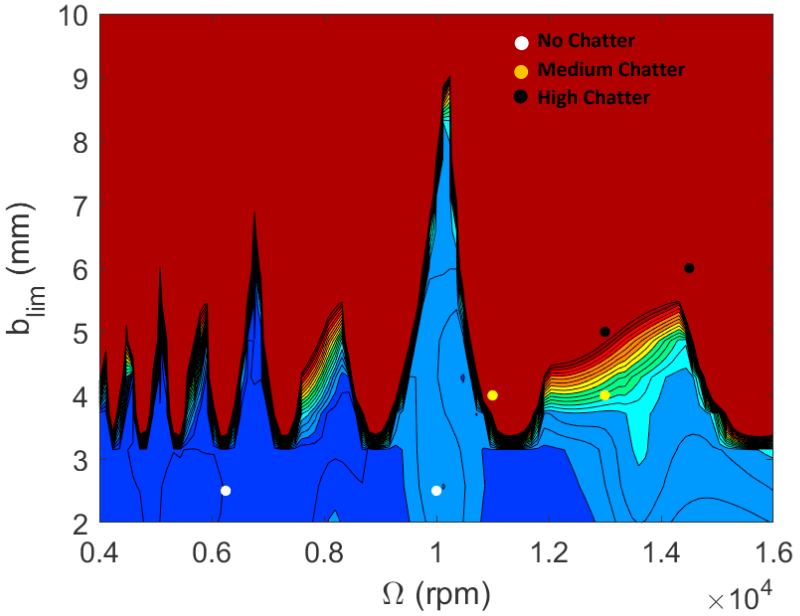

Fig. 5. Stability lobes

To compare the performance of EMD, EEMD, and VMD, chatter levels are specified as stable, medium, and high chatter. After the wavelet packet denoising process was performed, results were grouped into three per their chatter level. In Fig. 6, it is shown that the denoised signal and the raw signal for stabile and chatter situations. Before denoising outliners in collected signals are cleaned using Hampel filter. Afterward, the wavelet packet denoising process is performed by the 4th level and daubach3 function.

HHT images using the EMD process are given in Fig. 7. In the figure, there are two cuts at 14,500 rpm with a depth of cut of 6 mm and 7 mm. It has been observed that both of them are high chatter. The points at 11,000 and 13,000 rpm were chosen for the medium chatter at both 4 mm depth of cut. Also, for stable cut 2.5 mm is chosen as the minimum depth of cut. When the depth and rpm increase, results indicate a shift from stable to chatter state. On the Hilbert Spectrums of the selected cutting operations, color bar elevation from blue to yellow indicates the shift from stable to high chatter. The stable state has the largest frequency band. In transition, it becomes more greenish, and the frequency band becomes narrower. The high chatter data frequency band becomes even narrower, and the color code elevates to the maximum level. These bands can be seen in each IMF FFTs in Fig. 8, as well. FFT results of 2nd, 3rd, and 4th IMFs dominate HHT figures.

According to the FRF results, the peak modal values on the x-direction are 613, 953, and 2113 Hz. These frequencies are all marked with a red dot on the IMF plots. Frequencies intensify around the modal frequencies as expected [12, 29].

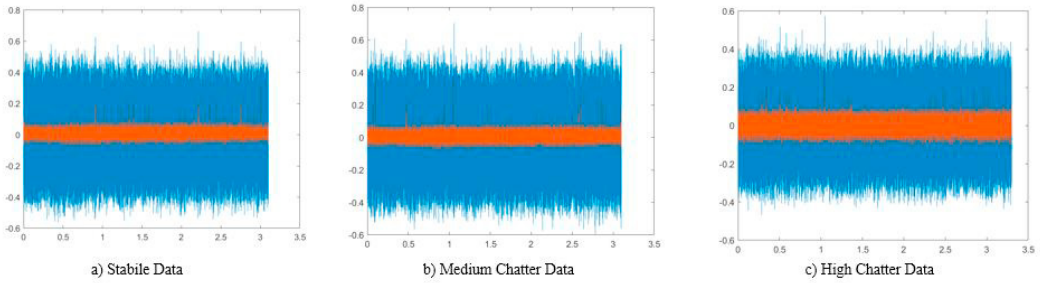

Fig. 6. Raw data and the denoised signal

a) Stable cut

b) Medium chatter cut

c) High chatter cut

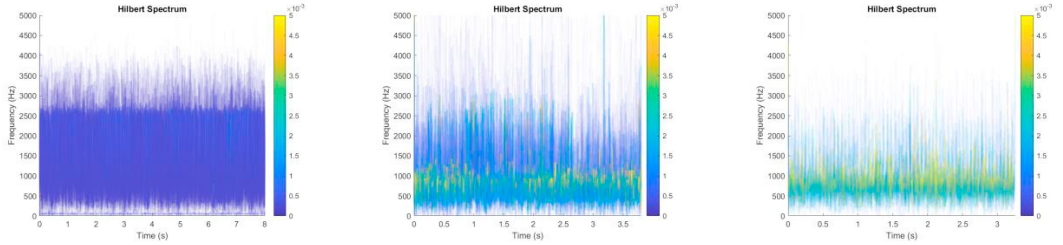

ω = 6250rpm, DOC = 2.5mm

ω = 13000rpm, DOC = 4mm

ω = 14500rpm, DOC = 7mm

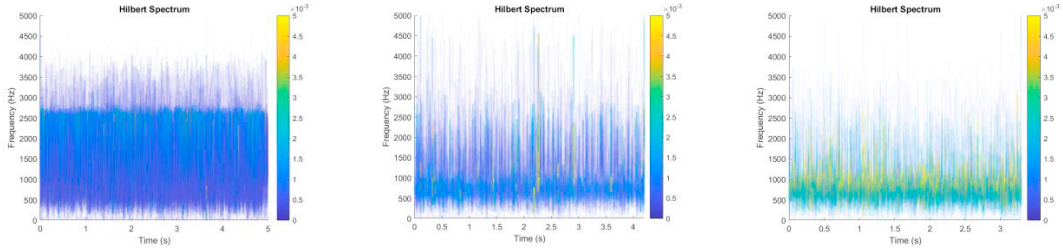

ω = 10000rpm, DOC = 2.5mm

ω = 11000rpm, DOC = 4mm

ω = 14500rpm, DOC = 6mm

Fig. 7. Hilbert transform of the vibration signals with EMD

a) Stable Data

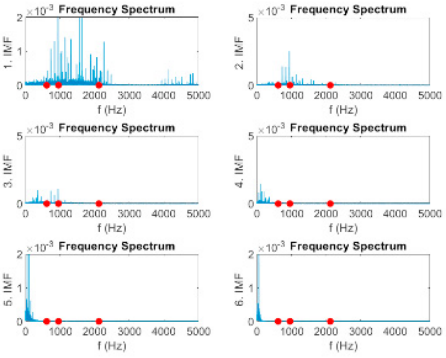

ω = 6250rpm, DOC = 2.5mm

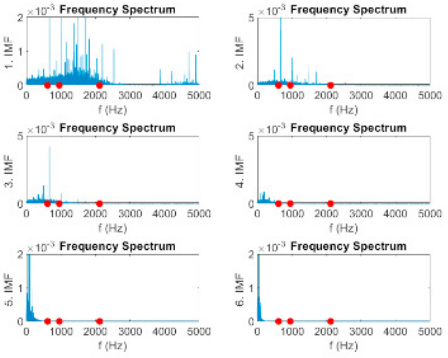

ω = 13000rpm, DOC = 4mm

b) Medium Chatter Data

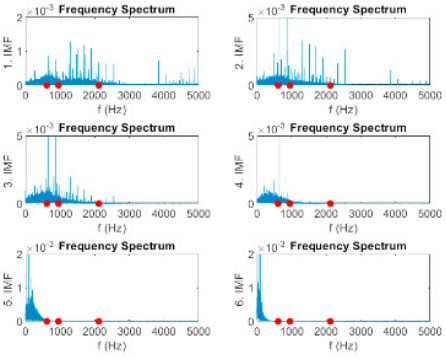

ω = 13000rpm, DOC = 4mm

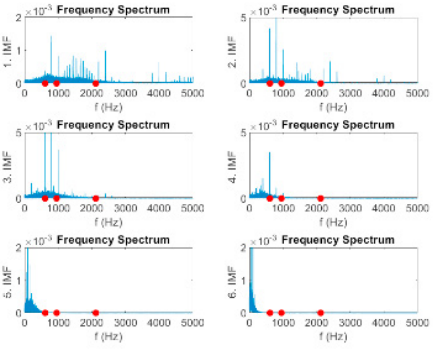

ω = 11000rpm, DOC = 4mm

c) High Chatter Data

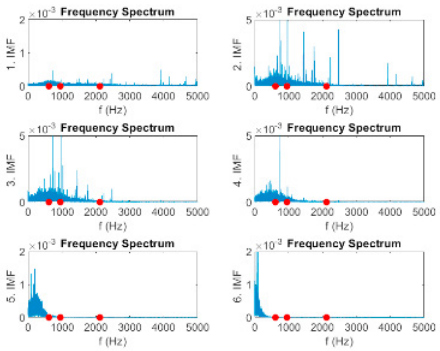

ω = 14500rpm, DOC = 7mm

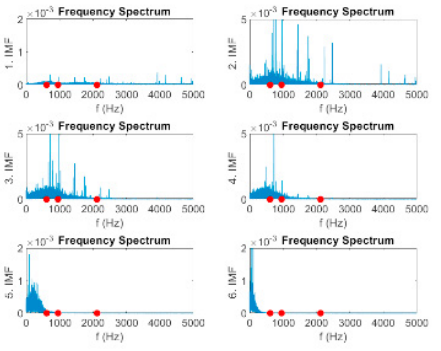

ω = 14500rpm, DOC = 6mm

Fig. 8. FFT of IMFs of the vibration signals with EMD

Secondly, HHT outputs using EEMD process results are given in Fig. 9. Interpretation of the EEMD results is similar to EMD results. The same color bar elevation and band getting narrower can be observed. Furthermore, the mode mixing problem is resolved in the cuts it occurred. Similar spectral behavior is also observed in Fig. 10. As the case shifts to chatter, the 2nd, 3rd, and 4th IMFs energy increases.

a) Stable data

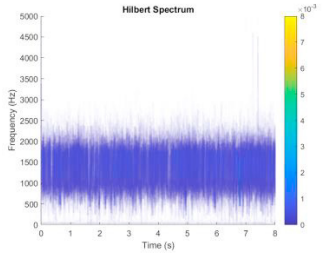

ω = 6250rpm, DOC = 2.5mm

b) Medium chatter data

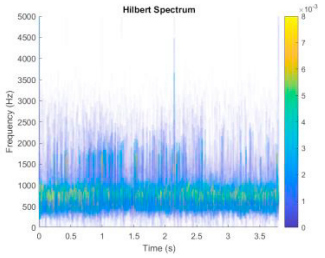

ω = 13000rpm, DOC = 4mm

c) High chatter data

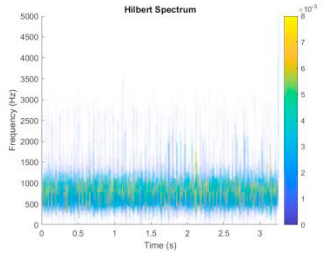

ω = 14500rpm, DOC = 7mm

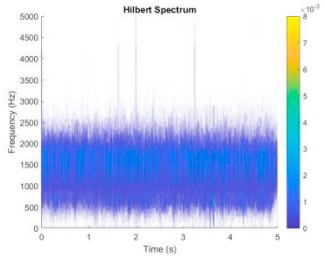

ω = 10000rpm, DOC = 2.5mm

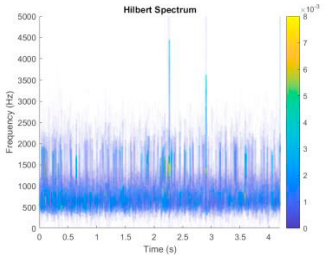

ω = 11000rpm, DOC = 4mm

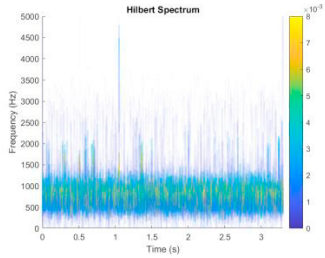

ω = 14500rpm, DOC = 6mm

Fig. 9. Hilbert transform of the vibration signals with EEMD

a) Stable cut

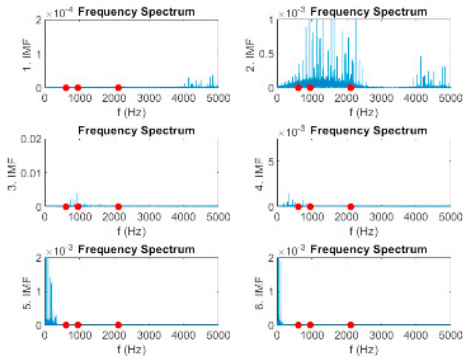

ω = 6250rpm, DOC = 2.5mm

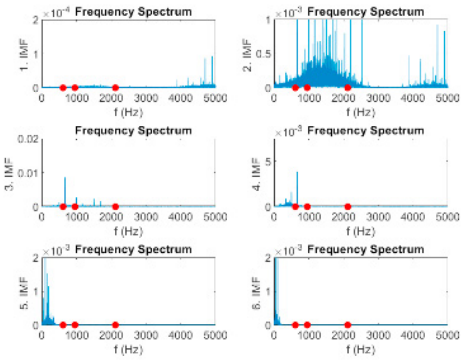

ω = 10000rpm, DOC = 2.5mm

b) Medium chatter cut

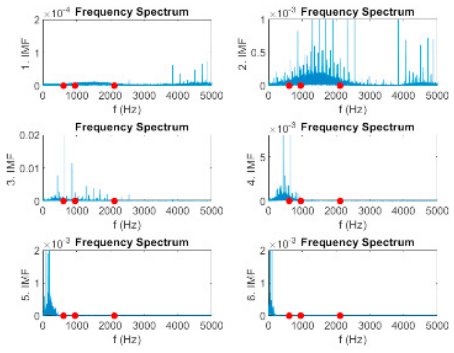

ω = 13000rpm, DOC = 4mm

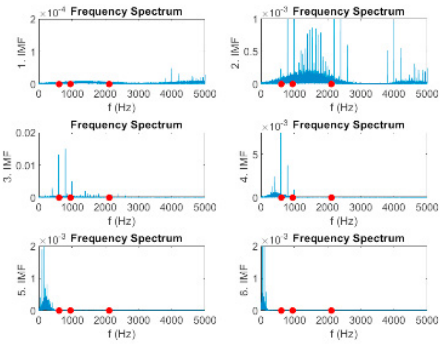

ω = 11000rpm, DOC = 4mm

c) High chatter cut

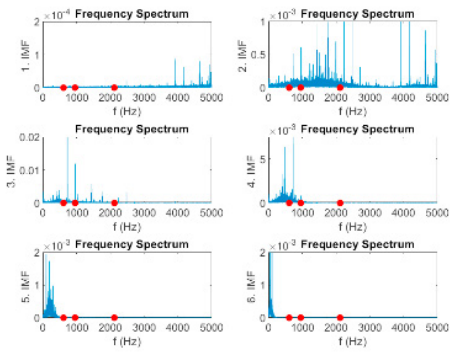

ω = 14500rpm, DOC = 7mm

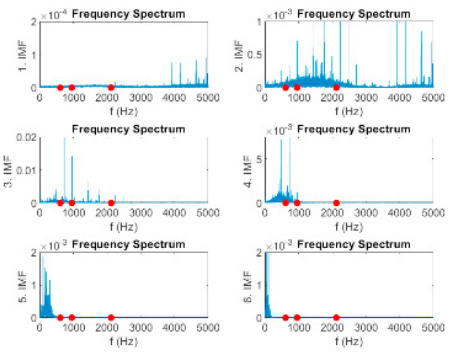

ω = 14500rpm, DOC = 6mm

Fig. 10. FFT of IMFs of the vibration signals with EEMD

Unlike EMD and EEMD, VMD separated the signals according to their frequencies. This distinction is obviously seen in both IMF FFTs and Hilbert spectrum results. In our analysis, the signal was decomposed into 6 IMFs. It is expected to see that the Hilbert spectrum has six separated frequencies. Fig. 11 shows that, from stable to chatter, around 750 Hz band color-code rise to yellow, and 1500 Hz weaker but still visible. All the other bands disappear in high chatter as these two bands dominate. Their increase can also be observed in IMFs in Fig. 12.

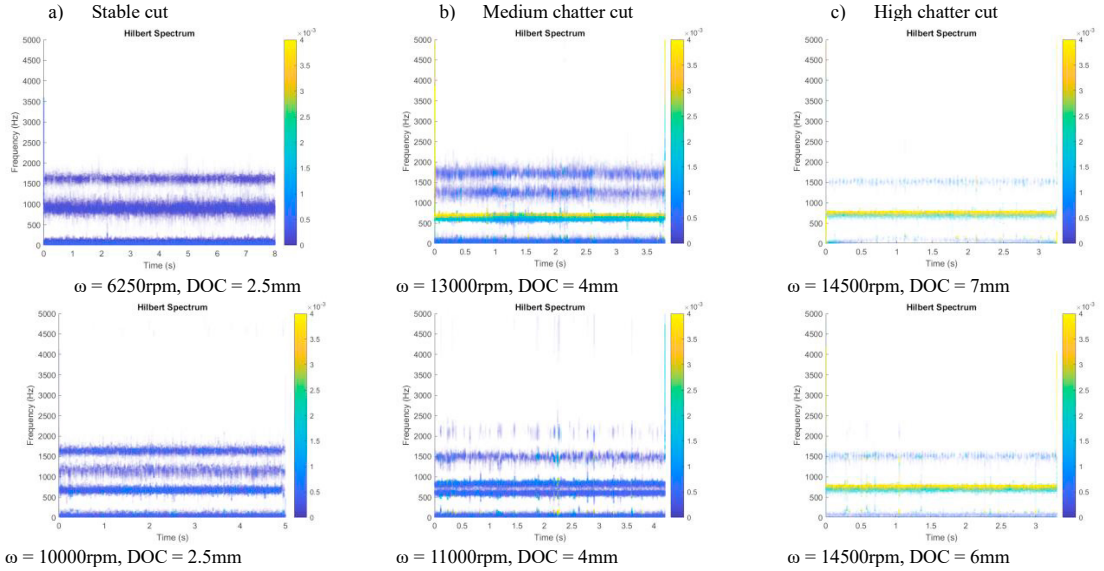

Fig. 11. Hilbert transform of the vibration signals with VMD

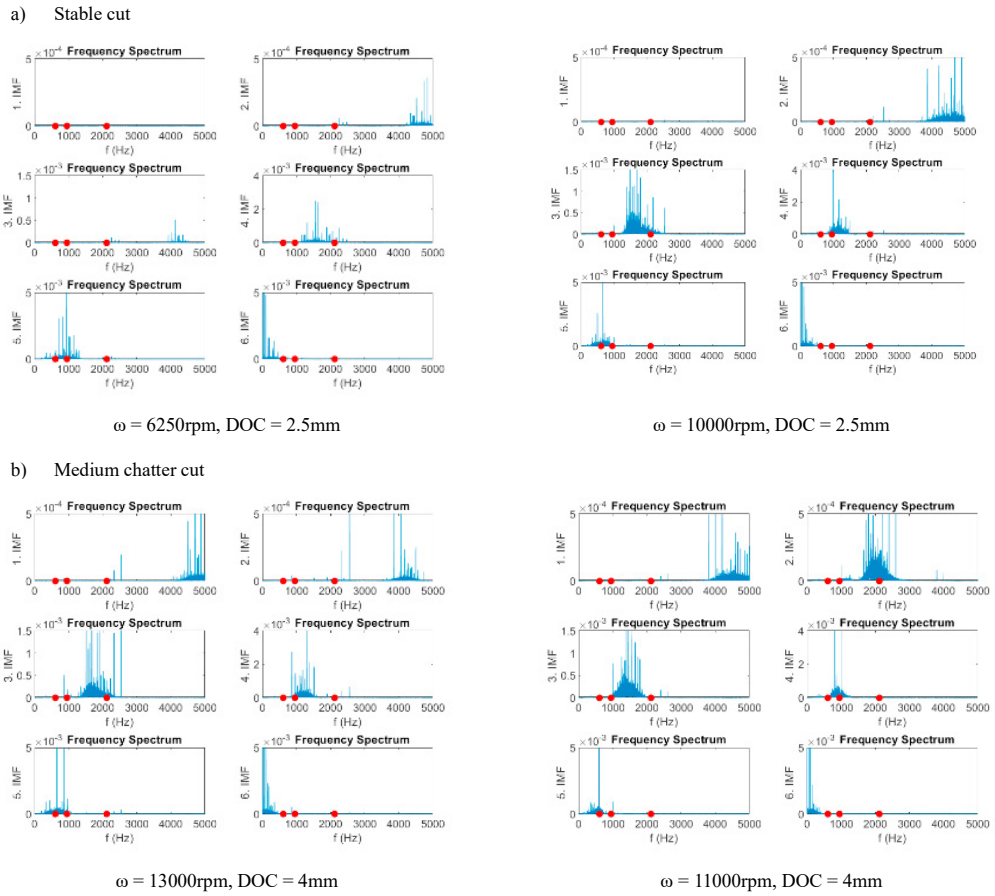

c) High chatter cut

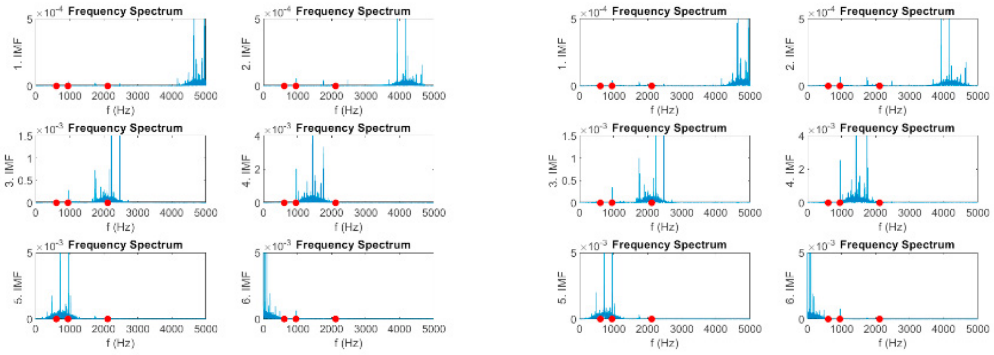

ω = 14500rpm, DOC = 7mm ω = 14500rpm, DOC = 6mm

Fig. 12. FFT of IMFs of the vibration signals with VMD

Finally, two of the cuts were selected, and EMD's entropy values were examined for each IMF. In the literature, it is stated that these values are the values representing the chatter. Fig. 13 clearly shows the increase in entropy values of the 2nd, 3rd, and 4th IMFs. The entropy results support the previous analyses on IMF and HHTs, as well. However, since these values vary according to rpm and depth of cut, they are not sufficient to interpret vibration signals, which are complex and time-varying signals. Therefore, and advanced time-frequency analysis such as Hilbert spectrum is essential for chatter identification.

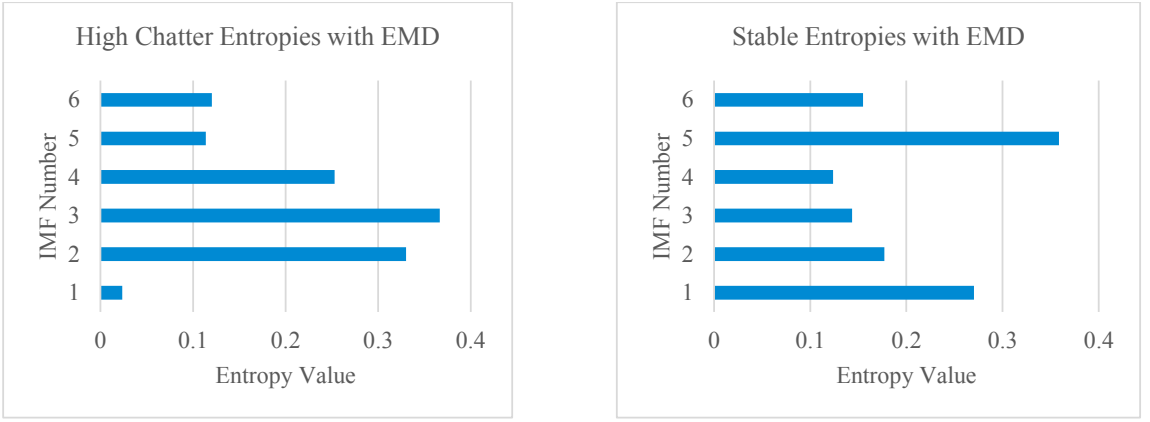

a) 14500 rpm and 6 mm DOC b) 6250 rpm and 2.5 mm DOC

Fig. 13. Entropies of each IMFs of EMD for stable and high chatter

4. Conclusion

In this study, the performance of HHT using three different mode decomposition methods, EMD, EEMD, and VMD, for chatter detection is analyzed and compared. Dataset was collected from a milling machine during the slot milling process. Before the process, the signals were denoised by Hampel filter and wavelet package denoising. In all methods, generated IMFs were investigated, and specific bands that exhibit an increase in generative chatter were chosen for Hilbert transformation.

It has also been experienced that the filter type and other methods for denoising should be carefully selected as its capability in reducing the noise but not remove the vital information in IMFs, is critical. Among the three mode decomposition methods, EEMD and VMD performed better and without problems compared to EMD. Hence it was concluded that they are the best candidates for intelligent chatter detection.

Acknowledgments

This study was funded by The Scientific and Technological Research Council of Turkey (TUBITAK) through project grant no. 118M414.

5. References

[1] Tlusty, J. and Ismail, F., (1983), “Special Aspects of Chatter in Milling”, Transactions of the ASME, Journal of Vibration Acoustics Stress and Reliability in Design, 105 (1): 24-32.

[2] Altintaş, Y. and Budak, E., (1995), “Analytical Prediction of Stability Lobes Milling”, Annals of CIRP, 44 (1): 357-362.

[3] Butcher, E.A., Nindujarla, P., Bueler, E., (2005), “Stability of Up- And Down-Milling Using Chebyshev Collocation Method”, Proceedings of IDECTC/CIE, ASME International Design Engineering Technical Conferences & Computers and Information in Engineering Conference, DETC2005-84880.

[4] Moghaddas, M., Ghaffari Saadat, M.H., (2007), “On The Investigation Of Machine Tool Chatter In The Milling Process”, Proceedings of IDECTC/CIE, ASME International Design Engineering Technical Conferences & Computers, and Information in Engineering Conference, DETC2007-35107: 2249-2255.

[5] Moradi, H., Movahhedy, M.R., Vossoughi, G., Ahmadian, M.T., (2011), “Investigation of the Internal Resonance and Regenerative Chatter Dynamics in Nonlinear Milling Process”, Proceedings of IDECTC/CIE, ASME International Design Engineering Technical Conferences & Computers and Information in Engineering Conference, DETC2011-48490.

[6] Kiss, A.K., Bachrathy, D., Stepan, G., (2016), “Surface Error and Stability Chart Of Beam-Type Workpiece In Milling Processes”, Proceedings of IDECTC/CIE, ASME International Design Engineering Technical Conferences & Computers and Information in Engineering Conference.

[7] Lamraoui, M., El Badaoui, M., Guillet, F., (2014), "Chatter detection in CNC milling processes based on wiener-SVM approach and using only motor current signals", Vibration Engineering and Technology of Machinery: pp 567-578.

[8] Wojciechowski, S., Maruda, R.W., Barrans, S., Nieslony, P., Krolczyk, G.M., 2017, (2017), "Optimisation of machining parameters during ball end milling of hardened steel with various surface inclinations", Elsevier, Journal of Measurement, (111): 18–28.

[9] Kuljanic, E., Totis, G., Sortino, M., (2009), "Development of an intelligent multisensor chatter detection system in milling", Mech. Syst. Sig. Process., 23(5):1704–1718.

[10] Penga, C. and Wanga, L., Liaob, T.W., (2015), "A new method for the prediction of chatter stability lobes based on dynamic cutting force simulation model and support vector machine", Science Direct, Journal of Sound and Vibration, 354: 118-131.

[11] Liu, C., Zhu, L., Ni, C., (2018), "Chatter detection in milling process based on VMD and energy entropy", Science Direct, Mechanical Systems, and Signal Processing, 105: 169-182.

[12] Cao, H., Lei, Y., He, Z., (2013), "Chatter identification in end milling process using wavelet packets and Hilbert–Huang Transform", International Journal of Machine Tools & Manufacture, 69: 11–19.

[13] Cao, H., Zhou, K., Chen, X., (2015), "Chatter identification in end milling process based on EEMD and nonlinear dimensionless indicators", International Journal of Machine Tools & Manufacture, 92: 52–59.

[14] Yang, K., Wang, G., Dong, Y., Zhang, Q., Sang, L., (2019), "Early chatter identification based on an optimized variational mode decomposition", Mechanical Systems and Signal Processing, 115: 238–254.

[15] Huang, N. E., Shen, Z., Long, S. R., Wu, M. L., Shih, H. H., Zheng, Q., Yen, N. C., Tung, C. C., Liu., H. H., (1998), "The empirical mode decomposition and Hilbert spectrum for nonlinear and nonstationary time series analysis", Proceedings of The Royal Society A Mathematical Physical and Engineering Sciences, 454(1971)

[16] Zeiler, A., Faltermeier, R., Keck, I. R., Tom´e, A. M., (2010) "Empirical Mode Decomposition - An Introduction", IEEE, International Joint Conference on Neural Networks (IJCNN).

[17] Ge, H., Chen, G., Yu, H., Chen, H., An, F., (2018), "Theoretical Analysis of Empirical Mode Decomposition", Journal of Symmetry, 10 (11).

[18] Huang, N.E., Wu, Z., (2009), “Ensemble Empirical Mode Decomposition: A Noise-Assisted Data Analysis Method”, World Scientific Publishing Company, 1(1):1–41.

[19] Gaci, S., (2016), “A new ensemble empirical mode decomposition (EEMD) denoising method for seismic signals”, Science Direct, Energy Procedia, 97: 84 – 91.

[20] Wanga, Y., Markertb, R., Xiangc, J., Zhenga, W., (2015), “Research on variational mode decomposition and its application in detecting a rub-impact fault of the rotor system”, Science Direct, Mechanical Systems and Signal Processing, 60-61: 243-251.

[21] Dragomiretskiy, K. and Zosso, D., (2013), “Variational Mode Decomposition”, IEEE Transactions on Signal Processing, 62 (3).

[22] Luo, G. and Zhang, D., (2012), “Wavelet Denoising”, Advances in Wavelet Theory and Their Applications in Engineering, Physics, and Technology.

[23] Lau, L., (2016), "Wavelet packets based denoising method for measurement domain repeat-time multipath filtering in GPS static high-precision positioning", GPS Solutions, 21 (2): 461-474.

[24] Kuzmanić, I. and Vujović, I., “Reliability and Availability of Quality Control Based on Wavelet Computer Vision”, SpringerBriefs in Electrical and Computer Engineering, 2015.

[25] Tikkanen, P.E., (1999), "Nonlinear wavelet and wavelet packet denoising of electrocardiogram signal", Biol Cybern, 80: 259–267

[26] Yu, J., Liu, D.C., (2008), "Thresholding-based Wavelet Packet Methods for Doppler Ultrasound Signal Denoising", 7th Asian-Pacific Conference on Medical and Biological Engineering, IFMBE Proceedings, Springer 19: 408-412.

[27] Walden, A.T. and Percival, D.B., (2000), “Wavelet Methods for Time Series Analysis”, Cambridge Series in Statistical and probabilistic mathematics.

[28] Souza, E. M, and Monico, J. F. G., (2004), "Wavelet Shrinkage: High-frequency multipath reduction from GPS relative positioning", GPS Solutions, 8(3):152-159.

[29] Altintaş, Y., (2012), “Manufacturing Automation”, Cambridge University Press.

[30] Zhang, Z., Li, H., Meng, G., Tu, X., Cheng, C., (2016) “Chatter detection in milling process based on the energy entropy of VMD and WPD”, International Journal of Machine tools and Manufacture, 108: 106-112.